NeuroImage 246 (2022) 118775

Contents lists available at ScienceDirect

NeuroImage

journal homepage: www.elsevier.com/locate/neuroimage

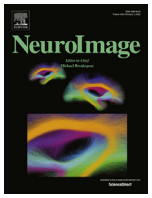

rPOP: Robust PET-only processing of community acquired heterogeneous amyloid-PET data

Leonardo Iaccarino[a], Renaud La Joie[a], Robert Koeppe[b], Barry A. Siegel[c], Bruce E. Hillner[d], Constantine Gatsonis[e,f], Rachel A. Whitmer[g,h], Maria C. Carrillo[i], Charles Apgar[j], Monica R. Camacho[k,l], Rachel Nosheny[k,m], Gil D. Rabinovici[a,n,*], for the Alzheimer's Disease Neuroimaging Initiative[#]

[a] *Memory and Aging Center, Department of Neurology, Weill Institute for Neurosciences, University of California San Francisco, San Francisco, CA, United States*
[b] *Department of Radiology, University of Michigan, Ann Arbor, MI, United States*
[c] *Edward Mallinckrodt Institute of Radiology, Washington University School of Medicine in St Louis, St Louis, MO, United States*
[d] *Department of Medicine, Virginia Commonwealth University, Richmond, VA, United States*
[e] *Center for Statistical Sciences, Brown University School of Public Health, Providence, RI, United States*
[f] *Department of Biostatistics, Brown University School of Public Health, Providence, RI, United States*
[g] *Division of Research, Kaiser Permanente, Oakland, CA, United States*
[h] *Department of Public Health Sciences, University of California Davis, Davis, CA, United States*
[i] *Medical and Scientific Relations Division, Alzheimer's Association, Chicago, IL, United States*
[j] *American College of Radiology, Reston, VA, United States*
[k] *San Francisco VA Medical Center, San Francisco, CA, United States*
[l] *Northern California Institute for Research and Education (NCIRE), San Francisco, CA, United States*
[m] *Department of Psychiatry, University of California San Francisco, San Francisco, CA, United States*
[n] *Department of Radiology and Biomedical Imaging, University of California San Francisco, San Francisco, CA, United States*

ABSTRACT

The reference standard for amyloid-PET quantification requires structural MRI (sMRI) for preprocessing in both multi-site research studies and clinical trials. Here we describe rPOP (robust PET-Only Processing), a MATLAB-based MRI-free pipeline implementing non-linear warping and differential smoothing of amyloid-PET scans performed with any of the FDA-approved radiotracers (^{18}F-florbetapir/FBP, ^{18}F-florbetaben/FBB or ^{18}F-flutemetamol/FLUTE). Each image undergoes spatial normalization based on weighted PET templates and data-driven differential smoothing, then allowing users to perform their quantification of choice. Prior to normalization, users can choose whether to automatically reset the origin of the image to the center of mass or proceed with the pipeline with the image as it is. We validate rPOP with n = 740 (514 FBP, 182 FBB, 44 FLUTE) amyloid-PET scans from the Imaging Dementia—Evidence for Amyloid Scanning – Brain Health Registry sub-study (IDEAS-BHR) and n = 1,518 scans from the Alzheimer's Disease Neuroimaging Initiative (n = 1,249 FBP, n = 269 FBB), including heterogeneous acquisition and reconstruction protocols. After running rPOP, a standard quantification to extract Standardized Uptake Value ratios and the respective Centiloids conversion was performed. rPOP-based amyloid status (using an independent pathology-based threshold of ≥24.4 Centiloid units) was compared with either local visual reads (IDEAS-BHR, n = 663 with complete valid data and reads available) or with amyloid status derived from an MRI-based PET processing pipeline (ADNI, thresholds of >20/>18 Centiloids for FBP/FBB). Finally, within the ADNI dataset, we tested the linear associations between rPOP- and MRI-based Centiloid values. rPOP achieved accurate warping for N = 2,233/2,258 (98.9%) in the first pass. Of the N = 25 warping failures, 24 were rescued with manual reorientation and origin reset prior to warping. We observed high concordance between rPOP-based amyloid status and both visual reads (IDEAS-BHR, Cohen's k = 0.72 [0.7–0.74], ~86% concordance) or MRI-pipeline based amyloid status (ADNI, k = 0.88 [0.87–0.89], ~94% concordance). rPOP- and MRI-pipeline based Centiloids were strongly linearly related (R^2:0.95, p<0.001), with this association being significantly modulated by estimated PET resolution (β= -0.016, p<0.001). rPOP provides reliable MRI-free amyloid-PET warping and quantification, leveraging widely available software and only requiring an attenuation-corrected amyloid-PET image as input. The rPOP pipeline enables the comparison and merging of heterogeneous datasets and is publicly available at https://github.com/leoiacca/rPOP.

* Corresponding author.
E-mail address: Gil.Rabinovici@ucsf.edu (G.D. Rabinovici).

[#] Data used in preparation of this article were obtained from the Alzheimer's Disease Neuroimaging Initiative (ADNI) database (adni.loni.usc.edu). As such, the investigators within the ADNI contributed to the design and implementation of ADNI and/or provided data but did not participate in analysis or writing of this report. A complete listing of ADNI investigators can be found at: http://adni.loni.usc.edu/wp-content/uploads/how_to_apply/ADNI_Acknowledgement_List.pdf

https://doi.org/10.1016/j.neuroimage.2021.118775.
Received 17 August 2021; Received in revised form 12 November 2021; Accepted 30 November 2021
Available online 7 December 2021.

1. Introduction

Positron emission tomography (PET) with specific radioligands can be used to measure brain amyloid plaque accumulation (amyloid-PET) in both clinical practice and research (Jagust, 2018; Villemagne et al., 2018). Three fluorine-18 radioligands are currently approved for clinical use by the U.S. Food and Drug Administration (FDA), i.e. ^{18}F-florbetapir (FBP, Amyvid^{TM}), ^{18}F-florbetaben (FBB, Neuraceq^{TM}) and ^{18}F-flutemetamol (FLUTE, Vyzamil^{TM}). With recent advances in disease-modifying treatments for Alzheimer's Disease (AD), amyloid-PET quantification has become standard in clinical trials, where it is used to screen eligible participants and evaluate drug or other intervention effects on amyloid plaques (Avgerinos et al., 2021). In future clinical uses, amyloid PET quantification may be needed to evaluate eligibility for drug therapy and gauge treatment response, e.g. to amyloid-beta targeting monoclonal antibodies (Mintun et al., 2021).

In most applications, amyloid-PET scans are processed and analyzed to obtain a global neocortical standardized uptake value ratio (SUVR), used to define amyloid status ($A\pm$) based on tracer- and method-specific thresholds. This approach requires the definition of reference and target regions-of-interest (ROIs), respectively, of areas devoid of specific binding (e.g., cerebellum for AD (Thal et al., 2002)), and of areas in which specific binding would indicate the ongoing disease process (e.g., frontal, parietal and temporal cortices for AD (Klunk et al., 2004)). A neocortical SUVR is then estimated as a target-to-reference ratio, which can subsequently be transformed to Centiloid units (Klunk et al., 2015), converting SUVRs across different methodologic approaches and radiotracers to a common scale, enabling comparison of data across different studies. The Centiloid scale is anchored at 0, which represents average binding in young cognitively-normal individuals who are highly unlikely to have amyloid deposition, and at 100, which represents average binding in individuals with mild-to-moderate dementia due to AD (Klunk et al., 2015).

The standard approach for amyloid-PET quantification relies on the processing of T1-weighted structural magnetic resonance imaging (MRI) acquired in proximity to amyloid-PET, given its higher resolution and anatomic definition compared to PET. This is the standard approach in multisite studies (e.g. the Alzheimer's Disease Neuroimaging Initiative [ADNI]), accompanied by additional processing to harmonize resolution of heterogeneous amyloid-PET scans, requiring participating sites to perform phantom PET scans (Jagust et al., 2015). While improving accuracy, MRI-based amyloid-PET processing adds cost, requires patients to undergo an additional scan and, depending on the quantification approach, can be computationally intensive and time-consuming. Moreover, requiring MRI-based processing prevents a patient with MRI contra-indications (e.g., certain pacemakers) from participating in multisite studies or clinical trials.

Several other PET-only processing pipelines, software and approaches have been described previously (Akamatsu et al., 2016; Bourgeat et al., 2015; Edison et al., 2013; Kang et al., 2018; Lilja et al., 2019; Lundqvist et al., 2013; Pegueroles et al., 2021). These include processing based on multi-atlas or adaptive PET templates, leveraging principal component analyses, deep learning and/or linear combination approaches (Akamatsu et al., 2016; Bourgeat et al., 2015; Fripp et al., 2008; Kang et al., 2018; Lilja et al., 2019; Lundqvist et al., 2013; Pegueroles et al., 2021). Other studies have also investigated canonical approaches to define tracer-specific PET templates, e.g. average of warped PET images, which were then used to drive spatial transformations (Bourgeat et al., 2015; Edison et al., 2013; Kang et al., 2018). Finally, several PET-only processing commercial and non-commercial software options are available, e.g. HERMES BRASS (Hermes Medical Solutions AB), Siemens Syngo.VIA Amyloid Plaque (Siemens Medical Solutions Inc.), PNEURO PMOD (PMOD Technologies Ltd), MIMNeuro (MIM Software Inc.), CortexID (GE Healthcare), Amyloid ^{IQ} (Invicro) and CapAIBL (Dore et al., 2016).

Here we present an open-source MRI-free pipeline (referred to as *rPOP,* robust PET-Only Processing, hereafter) which allows reliable, data-driven processing of community acquired heterogeneous amyloid-PET scans. rPOP was validated with all three FDA-approved tracers, is based on widely available software, is computationally efficient, includes data-driven differential smoothing and is fully automated. rPOP requires only an attenuation-corrected amyloid-PET scan acquired following manufacturer guidelines (i.e., appropriate acquisition time and radiotracer dose) and is publicly available at https://github.com/leoiacca/rPOP.

2. Materials and methods

rPOP involves two main processing steps: i) non-linear warping and ii) resolution estimation and differential smoothing. After running rPOP and subsequent necessary quality controls, rPOP users can proceed with their processing of choice, e.g. obtaining neocortical amyloid-PET SUVRs with ROIs in standard space (see Fig. 1 for a graphical summary).

Here we present and validate a standard approach where, using rPOP-warped and smoothed images, we quantify neocortical SUVRs using the standard Global Alzheimer's Association Interactive Network (GAAIN, http://www.gaain.org/centiloid-project) regions-of-interest (ROIs). Finally, for each of the three FDA-approved amyloid-PET tracers, we calibrate and obtain Centiloid scale conversion formulas.

2.1. Validation datasets

The first validation dataset included amyloid-PET scans performed with all 3 FDA-approved radiotracers in the Imaging Dementia—Evidence for Amyloid Scanning (IDEAS) Study (https://www.ideas-study.org/Original-Study). The IDEAS Study recruited more than 18,000 Medicare beneficiaries between February 2016 and January 2018, age 65 and older with either unexplained mild cognitive impairment (MCI) or dementia of uncertain cause (Rabinovici et al., 2019). The IDEAS dataset includes scans acquired at over 300 community-based PET facilities across the U.S., representing a wide variety of PET platforms, scanners and diverse acquisition and reconstruction protocols. We had access to a subset of IDEAS scans of participants who co-enrolled in the Brain Health Registry add-on study (IDEAS-BHR) (Nosheny et al., 2020), including $N = 740$ PET/CT attenuation-corrected amyloid-PET images (514, 182 and 44 using FBP, FBB and FLUTE, respectively). We defined amyloid status ($A\pm$) via rPOP-based Centiloid quantification (see details below) and an independently derived, pathology-based threshold of 24.4 Centiloids (La Joie et al., 2019). This approach was compared to amyloid status as defined by clinical visual reads performed at the respective IDEAS Study sites applying FDA-approved, radiotracer-specific criteria for clinical interpretations of amyloid PET (Rabinovici et al., 2019). All IDEAS-BHR participants had consented to be contacted regarding additional studies and provided electronic consent to be part of BHR and have such data cross-linked with the original IDEAS Study data (Nosheny et al., 2020). In the original IDEAS Study, written informed consent was obtained from all participants or their legally authorized representative (see details in (Rabinovici et al., 2019)).

As a secondary validation dataset, we downloaded all available baseline FBP- and FBB-PETs from the ADNI (adni.loni.usc.edu) database (as of December 2020), with a total of $N = 1{,}518$ scans (1,249 FBP and 269 FBB). The ADNI was launched in 2003 as a public-private partnership, led by principal investigator Michael W. Weiner, MD. The primary goal of ADNI has been to test whether serial MRI, PET, other biological markers, and clinical and neuropsychological assessment can be combined to measure the progression of MCI and early AD. For up-to-date information, see www.adni-info.org. All ADNI participants signed a written informed consent at the respective participating sites, see

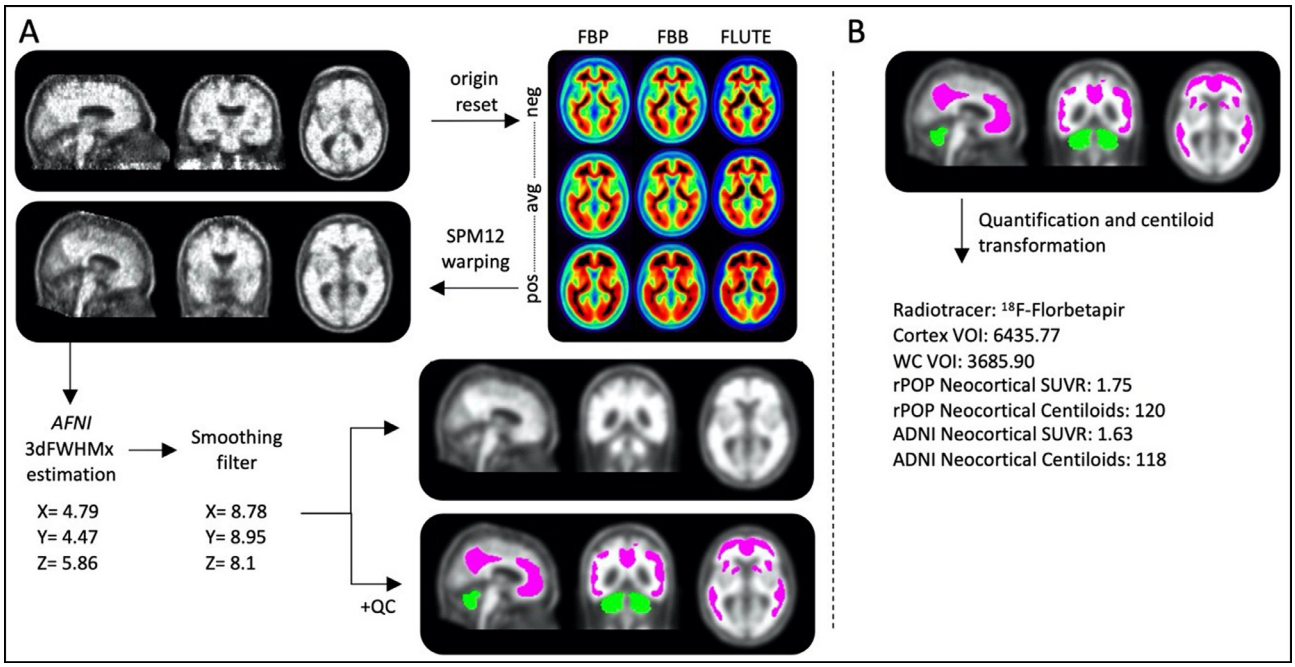

Fig. 1. Graphical summary of rPOP and quantification example.
Figure showing (A) a graphical summary of the rPOP pipeline and (B) an example of quantification using the Global Alzheimer's Association Interactive Network (GAAIN) 2mm regions of interest (cortex: purple, whole cerebellum: green) for an ADNI scan. rPOP-based PET Processing quantifications are compared to the ADNI MRI-based PET processing results for this specific case.

www.adni-info.org for details. See Supplementary Table 1 for a demographic and clinical summary for the two validation datasets.

ADNI images were more homogeneous with regards to the acquisition and reconstruction parameters, although acquired from five different scanner manufacturers and tens of scanner models. rPOP-based amyloid status and Centiloid units were cross-validated with ADNI Centiloids and $A\pm$ status as derived from the ADNI MRI-based PET processing and quantification pipeline (see (Jagust et al., 2015; Royse et al., 2021), ADNI documentation and below for details).

2.1.1. Dataset preparation

IDEAS-BHR dataset. DICOM datasets were downloaded as provided by the IDEAS Study Image repository and converted to NifTI with dicm2nii (https://github.com/xiangruili/dicm2nii) (Li et al., 2016). For cases in which the image set was uploaded by the site as a dynamic acquisition with multiple frames acquired during the imaging session, we rigidly realigned and averaged all the frames. No other image handling was performed before rPOP processing.

ADNI dataset. PET images in ADNI are pre-processed to various extents (Jagust et al., 2015). To be more comparable to the IDEAS-BHR dataset processing, we downloaded ADNI PET scans in their "Co-registered, Averaged" pre-processing stage (Step 2), i.e. without the differential smoothing performed in ADNI, in NIfTI format. No other image handling was performed before rPOP processing.

2.2. Software dependencies

- MATLAB (proprietary commercial software). rPOP has been validated with MATLAB R2018b (OS: macOS High Sierra) and R2020b (OS: macOS Mojave)
- Statistical Parametric Mapping v12 (SPM12) toolbox (publicly available) for MATLAB, available at https://www.fil.ion.ucl.ac.uk/spm/software/spm12/
- Analysis of Functional NeuroImages (AFNI) software suite (publicly available), downloadable at https://afni.nimh.nih.gov/. rPOP has been developed/validated with AFNI_20.3.03 (Dec 7 2020).

2.3. Spatial normalization

2.3.1. Templates generation

Three templates were generated for each FDA-approved radiotracer to represent a "negative", a "positive" and an "average" image. For both FBP-PET and FBB-PET we used $N = 100$ randomly selected ADNI images (50 amyloid-positive and 50 amyloid-negative, defined using ADNI MRI-based PET processing) in their fully preprocessed version (Step 4). 50 positive and 50 negative scans were used to create the "positive" and "negative" tracer-specific templates, while the 100 images were combined to generate the "average" template for each tracer. For FLUTE-PET, we used the GAAIN dataset, which includes $n = 50$ participants with likely high amyloid burden (i.e., including dementia due to AD, amnestic MCI and older healthy controls (>45 yrs old)) and $n = 24$ younger healthy controls. All 74 scans were used to generate the "average" template. We then applied the GAAIN Centiloid values to split the FLUTE-PET dataset and generate the "negative" and "positive" templates based on an a priori threshold of 24.4 Centiloids (La Joie et al., 2019).

All templates were generated with the same standard approach, including i) PET-to-MRI rigid-body co-registration, ii) non-linear warping of the MRI to the standard space, iii) application of transformation parameters to the registered PET scans, iv) calculation of a soft mean of the warped PET scans to create the template image. All the templates are available at: https://neurovault.org/collections/CPHVNXDQ/ (see also Fig. 1A and Supplementary Figure 1) and on https://github.com/leoiacca/rPOP.

2.3.2. Non-linear warping

At the beginning, rPOP prompts the user to indicate whether automatic origin resetting to the center of the image should be performed. Resetting the origin greatly improves the precision of warping and is recommended unless the field of view during the acquisition was particularly large (e.g. including whole neck), or in case the origin of the input scan has been already manually set. Extra care is needed for images with pronounced head tilting or subject misposi-

tioning, although a failed warping would be noticed in the later QC phases. The code performing the origin reset is from F. Yamashita and is part of an ac/pc co-registration script (parent function available at: http://www.nemotos.net/scripts/acpc_coreg.m).

Next, the user is asked to choose which PET templates to use for the non-linear warping. rPOP comes with two main options, i.e., tracer-independent and tracer-dependent. In the tracer-independent approach, all nine PET templates (3 for each tracer) will be entered at the same time in the computation for any given scan. In the tracer-dependent approach, the user is instead asked to choose which set of templates to use based on the tracer. rPOP was originally designed to run with a tracer-independent approach to allow users to begin spatial processing of PET scans even when lacking or doubting radioligand information, e.g., with initial large data transfers, lacking clear metadata etc. Using all nine amyloid-PET templates may also allow a more efficient handling of atypical binding patterns. In both approaches, using either nine (tracer-independent approach) or three (tracer-dependent approach) templates, SPM12 will try "to find the best linear combination of these images [i.e., the templates] in order to best model the intensities in the source image" (see SPM12 manual at https://www.fil.ion.ucl.ac.uk/spm/doc/spm12_manual.pdf). Therefore, regardless of the number of templates used, SPM will first derive a linear combination, and then use the combined image to drive spatial normalization. Non-linear warping in rPOP is performed using the SPM12 *Old Normalization* toolbox, using default settings except for the bounding box, which was modified to be larger, i.e. [−100 −130 −80; 100 100 110].

2.4. Full-width at half maximum (FWHM) estimation and differential smoothing

After warping, rPOP uses the AFNI (Cox, 1996; Cox and Hyde, 1997) *3dFWHMx* function (see details at https://afni.nimh.nih.gov/pub/dist/doc/program_help/3dFWHMx.html) to estimate the Full-Width at Half-Maximum (FWHM) differential smoothing kernel to be applied to the individual scan. The call includes flags to enable automated computation of a brain mask (*-automask*) and to model the intrinsic spatial structure of the signal in the PET image (*−2difmad*). Estimated FWHMs are saved in text files for each scan and automatically imported into MATLAB. Based on the estimations, the resulting smoothing filter is calculated based on the standard formula for each plane:

$$filter = \sqrt{(FWHM_{target})^2 - (FWHM_{estimated})^2}$$

In rPOP the target resolution is set to an approximate isotropic 10mm^3 resolution, as this was the 80th percentile of the FWHM estimations in the IDEAS-BHR dataset (see also below). This dataset was chosen as a reference to define the target resolution given that it is more representative of community acquired scans, with a wider range of image quality and resolution. For each given image and plane, in case the estimated FWHM was higher than target resolution, then the assigned smoothing filter would be 0. Smoothing of the image based on the defined filters was then applied with SPM12 with default parameters.

To validate the accuracy of 3dFWHMx in estimating the FWHM, we used a dataset of $N = 158$ warped ^{11}C-PiB-PET scans (included in (Iaccarino et al., 2021)), acquired at the Lawrence Berkeley National Lab (Berkeley, CA, USA) on a Siemens Biograph 6 Truepoint PET/CT scanner in 3D acquisition mode. The calculated image resolution for these scans is 6.5 × 6.5 × 7.25 (average 6.75) mm using a Hoffman phantom. Comparing the average estimated FWHM for each of these scans to the average calculated resolution resulted in high accuracy, with an average±sd absolute FWHM estimation error of 0.39±0.33mm^3. The same validation was performed on a subset of $N = 280$ (of which, 255 FBP-PET and 25 FBB-PET) scans from the ADNI dataset (as it was the largest group with the same scanner, i.e. Siemens ECAT Exact HR+), with a similar error of 0.44±0.4mm^3.

2.5. Quality control

Controlling the accuracy of the non-linear warping is essential to determine the reliability of the subsequent quantification. It is strongly recommended that single-subject QC be performed, including at least a qualitative evaluation of each non-linearly warped image to assess the accuracy of the spatial transformation. Orientation and size should match template space and there should not be macroscopic artifacts or deformations in the brain, with special attention to the reference region. In case the user chooses to proceed with an ROI-based analysis (as presented below), it is critical at this stage to assess the goodness of fit of the quantification ROIs on each warped image. Examples of this QC process performed with the *slover* SPM12 function are shown in Fig. 2A, using the GAAIN 2 mm reference (whole cerebellum) and target regions.

In case macroscopic distortions in the warped images ("hard" failures) are detected, rPOP should be re-run after manually reorienting and resetting the origin to assist the non-linear warping. In case the resulting warping is still not accurate, it is likely that some features in the image hamper the spatial normalization, and the user should consider more advanced image preprocessing (e.g., cleaning extra-brain tissue, cropping) or ultimately dropping the scan from analysis.

2.6. Quantification example: estimation of neocortical SUVR and Centiloids

As a quantification example, here we quantified neocortical SUVRs by using the GAAIN 2 mm cortical and whole cerebellar ROIs (respectively, target and reference). We also obtain tracer-specific Centiloid conversion formulas for each of the FDA-approved radioligands, following the process outlined in the Centiloid methods paper (Klunk et al., 2015). Level 1 and 2 Centiloid calibration data are available in the Supplementary material.

Based on the calibration, the following formulas were estimated to convert rPOP-based neocortical SUVRs to rPOP-based Centiloids:

$$FBPCL = (189.9 * FBPSUVRind) - 211.1$$
$$FBBCL = (160.7 * FBBSUVRind) - 169.2$$
$$FLUTECL = (127.6 * FLUTESUVRind) - 136.2$$

These conversion formulas are specific to the default processing described above. Any methodological variation would invalidate the formulas and require the user to cross-validate or recalibrate the processing accordingly.

2.7. Data/code availability statement

Both IDEAS and ADNI data are available conditional to approval of a data request to be submitted through the respective websites, at https://www.ideas-study.org/Original-Study/Data-Request and at http://adni.loni.usc.edu/data-samples/access-data/. Source code for rPOP is available at https://github.com/leoiacca/rPOP.

3. Results

3.1. IDEAS-BHR dataset

At visual inspection of rPOP-processed IDEAS-BHR images, we identified macroscopic warping failures for 10/740 (1.35%) images. For 9/10 of the failures, manually resetting origin and orientation prior to the non-linear warping was enough to troubleshoot. The only unrecovered failed scan had very intense meningeal uptake, which may have hampered the warping estimations (see Supplementary Figure 2). Examples of warped scans are available in Fig. 2a. Supplementary Figure 3 shows examples of successful warping in scans with atypical features from the IDEAS-BHR dataset. The 3dFWHMx resolution estimations are summarized in Supplementary Table 2 and were heterogeneous (mean±sd FWHM across the three planes: 8.63±1.73, range 3.7–15.18).

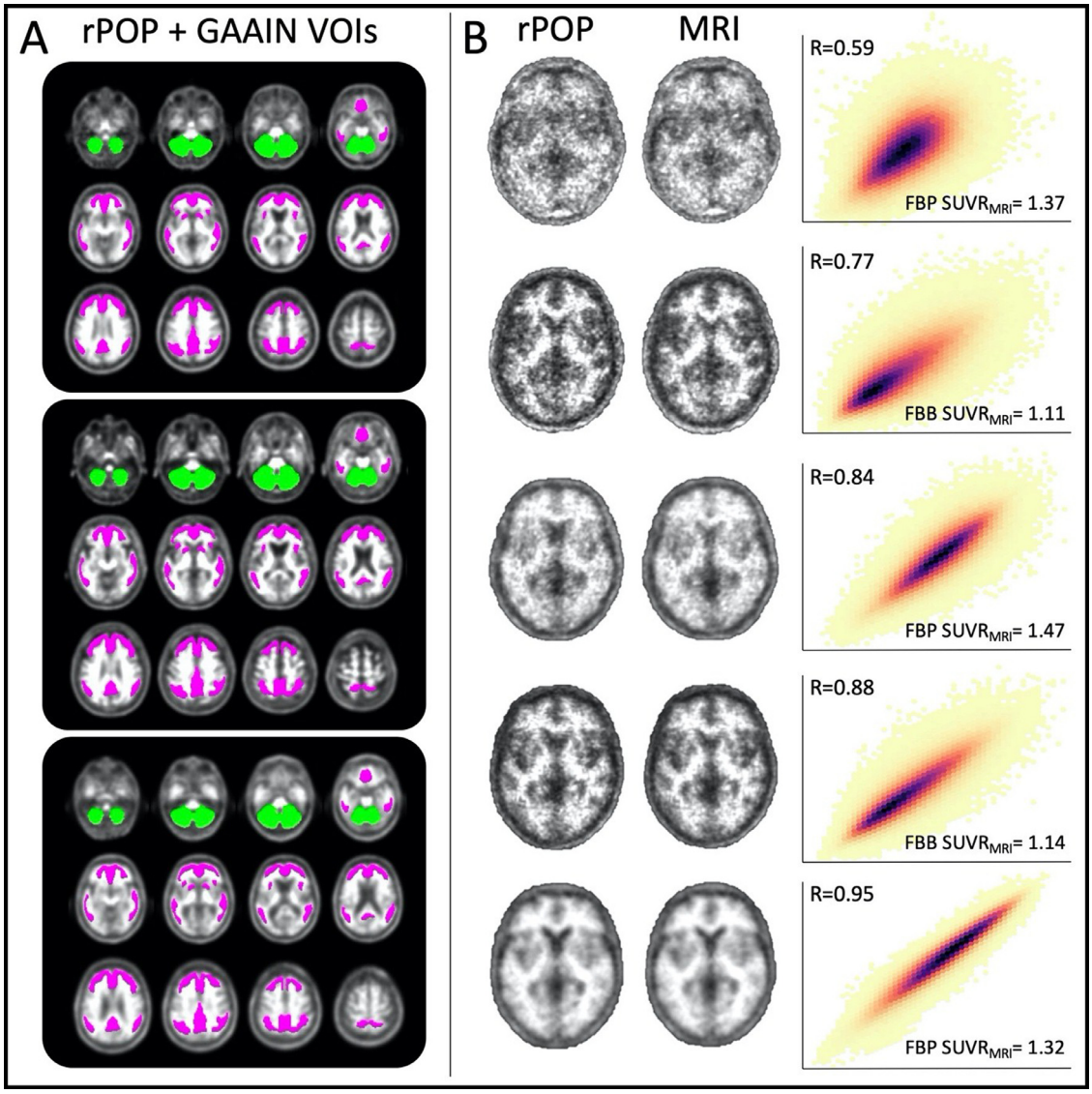

Fig. 2. Quality control of rPOP non-linear warping.
Figure showing examples of quality control of rPOP-based non-linear warping. Panel (A) shows three random scans from the IDEAS-BHR dataset, warped and smoothed with rPOP, with the GAAIN 2 mm ROIs overlaid (cortex: purple, whole cerebellum: green). Panel (B) shows five ADNI amyloid-PET scans warped either via rPOP or via the standard MRI-based approach, with the respective voxelwise linear correlation and hexed scatterplot. These scans were selected according to the magnitude of the correlation, representing the minimum, 2nd quintile, median, 4th quintile and maximum correlations. Additional examples for different degrees of positivity are available in Supplementary Figure 8. See text for details.

Differential smoothing examples are provided in Supplementary Figure 4.

Amyloid-PET visual reads and disease stage (MCI or dementia) were available for 663/739 warped and valid scans. Of these 663 scans, 12 were judged to have suboptimal warping quality at QC, most involving a "stretching" artifact in the cerebellum, brainstem and midbrain (see Supplementary Figure 5). rPOP-based amyloid status showed agreement with local radiologist's visual reads in IDEAS, with 86% concordance and a Cohen's k of 0.72 (0.70|0.74, substantial agreement). Most of the discordances (61/91, 67%) were rPOP-based A- vs. local visual read *A*+ cases, suggesting that rPOP quantification (with the 24.4 a priori Centiloid threshold) was more conservative. Results were identical when removing the 12 cases with suboptimal warping quality (see Table 1 and Fig. 3A for a summary).

When stratifying according to clinical stage (either MCI or dementia), we observed the expected Centiloids distribution, with an average of 2 ± 23 and −5 ± 27 Centiloids in A- MCI and dementia participants (respectively, based on visual read), and an average of 65±42 and 80±37 Centiloids in *A*+ MCI and dementia participants (respectively). See Table 2 and Fig. 3A for details.

3.2. ADNI dataset

Visual inspection of rPOP-processed ADNI images identified 15/1,518 (0.99%) warping failures on single-subject QC. All the failures were rescued when reorienting and resetting the origin manually. The 3dFWHMx estimations are summarized in Supplementary Table 2. Overall, ADNI scans appeared to have a higher estimated resolution (lower FWHM) compared to IDEAS-BHR scans (mean±sd 5.67±1.77 and 8.63±1.73, respectively, effect size Cohen's d = 1.68, p<0.001). rPOP-based Centiloids and *A*± status (Centiloids≥24.4) were compared with ADNI MRI-based neocortical Centiloids, and *A*± status, defined according to tracer-specific thresholds used in ADNI, i.e. >20 Centiloids for FBP-PET and >18 Centiloids for FBB-PET (Royse et al., 2021). Com-

Table 1
Agreement of rPOP-based amyloid status definition.

Cohort	IDEAS-BHR	ADNI
Comparison Standard	Local visual reads	ADNI A± Centiloids>18 FBB Centiloids>20 FBP
Total (N)	663	1518
rPOP *A*+ | Comp. Standard *A*+ (N)	328	704
rPOP A- | Comp. Standard A- (N)	244	725
rPOP *A*+ | Comp. Standard A- (N)	30	10
rPOP A- | Comp. Standard *A*+ (N)	61	79
Overall agreement (%)	86	94
Cohen's κ	0.72 (0.70–0.74)	0.88 (0.87–0.89)

Legend: *N*=Number, Comp. Standard=Comparison Standard, A-=Amyloid-Negative; *A*+=Amyloid-Positive, FBP=18F-florbetapir, FBB=18F-florbetaben.

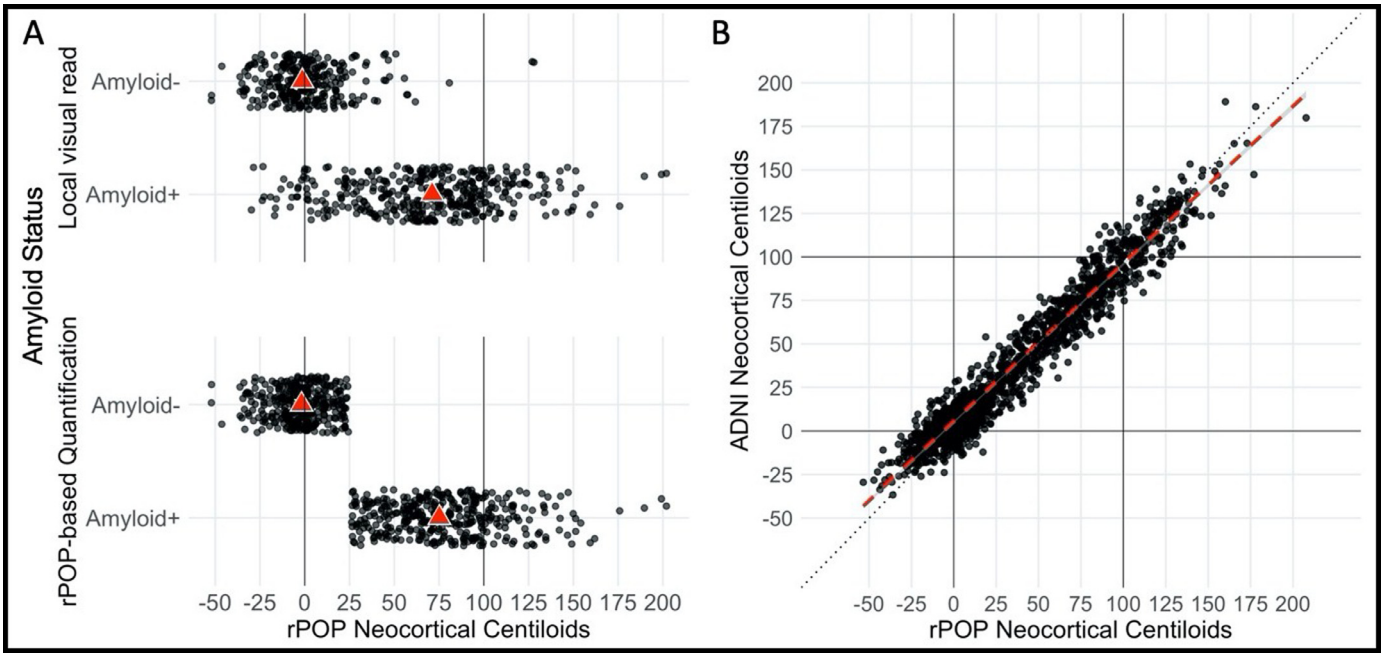

Fig. 3. rPOP-based Centiloids distribution.
Figure showing distributions of rPOP-based Centiloids. Panel A shows jittered dotplots demonstrating distribution of rPOP-based Centiloid values in the IDEAS-BHR dataset according to two different standards, i.e. local visual reads (top) or rPOP-based Quantification (>24.4 Centiloids, bottom). Panel B shows a dispersion scatterplot demonstrating the linear association between rPOP-based and MRI-based Neocortical Centiloid values in the ADNI dataset. Black dotted line represents identity, the red dashed line indicates linear fit. For both panels, gridlines corresponding to Centiloid values of 0 and 100 are bolded.

Table 2
Centiloid values summary.

Dataset	IDEAS-BHR (*N* = 663)		ADNI (*N* = 1518)	
Amyloid Status Method	Local visual read	rPOP-based quantification	MRI-based quantification	
Centiloid Method	rPOP-based PET Processing		rPOP-based PET Processing	MRI-based PET Processing
CN (A-)	–	–	−2 (13)	2 (9)
MCI (A-)	2 (23)	−2 (15)	−3 (14)	0 (10)
Dementia (A-)	−5 (27)	−6 (19)	−8 (16)	−4 (13)
CN (A+)	–	–	53 (32)	55 (31)
MCI (A+)	65 (42)	75 (33)	72 (35)	72 (33)
Dementia (*A*+)	80 (37)	86 (30)	89 (33)	86 (31)

All values are expressed as mean(sd).
Amyloid status was defined differently across datasets given that visual reads are not available in ADNI. For the IDEAS-BHR data, summary values per clinical group are provided also according to amyloid status defined with the rPOP-based Centiloids and the a priori 24.4 threshold. For the ADNI dataset, Amyloid status was uniquely defined as provided by ADNI, which is based on MRI-based PET quantification and tracer-specific thresholds (see text for details). In the ADNI dataset, summary values are provided for both rPOP-based and MRI-based PET Processing-derived Centiloids.
Legend: CN=Cognitively Normal; MCI=Mild Cognitive Impairment; A- =Amyloid-Negative; *A*+ =Amyloid-Positive.

pared to the ADNI approach valuing sensitivity, our singular 24.4 Centiloid cut-off approach is slightly more restrictive and thus more conservative in defining $A\pm$ status. rPOP-based $A\pm$ status was highly concordant with ADNI $A\pm$ status, with 94% agreement and a Cohen's k of 0.88 (0.87|0.89, almost perfect agreement) (see Table 1). Most of the observed discordances included scans defined as rPOP A- and as ADNI $A+$. Given that different Centiloids threshold were used (24.4 for rPOP, 18/20 for FBB/FBP in ADNI), analyses were repeated also comparing rPOP-based $A\pm$ with ADNI $A\pm$ using instead the same 24.4 Centiloids threshold (applied to the ADNI MRI-based PET Processing), which resulted in improved agreement (96% concordance, Cohen's k 0.93, 0.92|0.93). When stratifying according to amyloid status and clinical diagnosis (either cognitively normal, MCI or dementia), we observed the expected increase in rPOP-based Centiloids distribution based on clinical stage, consistent with the MRI-processing derived ADNI Centiloids and with the distribution in the IDEAS-BHR dataset (see Table 2). To further investigate the impact of different Centiloid thresholds on the agreement between rPOP-based and ADNI-based $A\pm$ status, we estimated overall concordance and Cohen's k across a wider range of thresholds, i.e. from 1 to 100 Centiloids with increments of 1 Centiloid (total of 100 thresholds). Overall concordance range was 0.85–0.97, median 0.96, being highest with thresholds between 25 and 50 Centiloids. Cohen's k range was 0.62–0.93, median 0.89, being also highest with thresholds between 25 and 50 Centiloids (see Supplementary Figure 6).

In a univariate linear model, rPOP-based Centiloids were highly correlated with ADNI Centiloids (R^2:0.95, $p<0.001$, slope: 0.91, intercept 5.14, see also Fig. 3B). There was no interaction with tracer ($\beta = -0.003$, $p = 0.86$), whereas there was a significant interaction between estimated FWHM and rPOP Centiloids in correlations with ADNI Centiloids ($\beta = -0.016$, $p<0.001$). Overall, with lower resolution of the input scans, rPOP Centiloids tended to slightly under-estimate ADNI Centiloids in the most negative range and over-estimate in the most positive range (see Supplementary Figure 7). Finally, the deviation between rPOP- and MRI-based PET-processing Centiloids was not strongly associated with amyloid burden ($r = 0.19$), suggesting rPOP performs similarly across the range of amyloid positivity.

As an additional validation, we estimated spatial correlation between amyloid-PET images warped via either MRI-based or rPOP-based transformation parameters. Spatial correlation is estimated by calculating correlation coefficients, for each given pair of scans and across all voxels, restricting the analysis to the cortical gray matter (Bejanin et al., 2019). We selected a random subset of 200 scans (100 FBP and 100 FBB) with available MRI from the ADNI dataset. Excluding one MRI-based warping failure, we observed overall strong correlations, with an average correlation coefficient of 0.83 (±0.07, range 0.59–0.95). See Fig. 2B and Supplementary Figure 8 for representative examples. As further validation of the rPOP-based warping accuracy, we also estimated regional-level correlations between SUVR values extracted from images warped via either MRI-based or rPOP-based transformation parameters. To do so, we selected the $N = 199$ ($N = 99$ FBP, $N = 100$ FBB) scans from the spatial correlation analysis, considering both their MRI-based and rPOP-based warped versions ($N = 398$ scans total) and intensity normalized all of them using the same reference region, i.e. the GAAIN whole cerebellar ROI. We then proceeded to extract average regional SUVR values (considering only positive voxels to avoid bias due to field of view cut) using definitions from the Neuromorphometrics Atlas distributed with SPM. The Neuromorphometrics tissue labels are based on MRI scans from the OASIS project (https://www.oasis-brains.org/) and are provided by Neuromorphometrics Inc. under academic subscription (see also SPM12 Release Notes at https://www.fil.ion.ucl.ac.uk/spm/software/spm12/SPM12_Release_Notes.pdf). The Neuromorphometrics atlas includes $N = 136$ regional definitions, of which we selected $N = 126$ of interest, excluding CSF, ventricles, optic chiasm and vessels. The analysis demonstrated very high average correlation coefficients across the different regions, for both tracers (range 0.69–0.99, median 0.95 for FBP; 0.6–0.99, median 0.94 for FBB). See also Supplementary Tables 3–4 for details.

4. Discussion

Here we present and validate rPOP, an MRI-free MATLAB-based pipeline to achieve accurate amyloid-PET quantification requiring only an attenuation-corrected amyloid-PET image as input. rPOP provides a PET-only processing alternative to MRI-reliant methods of amyloid PET quantification (and to expensive clinical quantification software packages), applying a unified approach to i) non-linearly warp amyloid-PET images to template space and ii) bring them to a common resolution. Here we show that rPOP-based amyloid status was highly concordant with amyloid status based on two different comparison standards, local visual reads at the clinical sites using FDA-approved criteria (IDEAS-BHR dataset) or quantification derived from MRI-based PET processing (ADNI dataset). rPOP-based Centiloids were strongly linearly associated with MRI-dependent-pipeline derived Centiloids, with rPOP- and MRI-based warped amyloid-PET images being on average highly spatially similar.

Distinct from previous PET-only approaches (Akamatsu et al., 2016; Bourgeat et al., 2015; Edison et al., 2013; Fripp et al., 2008; Kang et al., 2018; Lilja et al., 2019; Lundqvist et al., 2013; Pegueroles et al., 2021) and available commercial/non-commercial software, rPOP combines: i) a multi-atlas approach with a subject-specific linear combination component; ii) validation performed on the three different FDA-approved radiotracers; iii) validation based on highly heterogeneous, community acquired data; iv) both MRI-based quantification and visual clinical reads comparison standards; v) a data-driven component of differential smoothing to support harmonization of resolution across different sites and scanners; and vi) an open-source distribution.

To be considered accurate in most clinical scenarios, rPOP was validated on thousands of amyloid-PET scans from two very different cohorts. The heterogeneous IDEAS-BHR scan collection can be considered as one of the most representative community-level amyloid PET datasets currently available. The ADNI dataset, although heterogeneous from the scanner manufacturer/model standpoint, presents with more homogeneous scan quality and acquisition protocols. rPOP performed well in both datasets, validating the resulting amyloid-status using two different, dataset-specific comparison standards. In the IDEAS-BHR dataset, rPOP converged with local visual reads also in the context of remarkably heterogeneous community acquired scans. The present findings thus show that amyloid status estimated through rPOP converges with MRI-derived PET processing or visual reads in the great majority of cases. We also show that scan resolution significantly impacts the precision of rPOP-based Centiloid values, and thus users should be particularly cautious when processing amyloid-PET scans with lower resolutions in rPOP. The accuracy of rPOP amyloid status estimation is tightly associated with, and dependent on, a thorough quality control of the non-linear warping. Considering our quantification approach, the reliability of the analysis depends on the goodness of fit of the target and reference region ROIs on the warped images, and users are thus strongly encouraged to implement their single-subject quality control approach of choice.

Amyloid PET quantification may be increasingly important in clinical practice given recent advances in molecular-specific therapies for AD. Aducanumab, an amyloid-beta targeting monoclonal antibody, was recently granted accelerated approval by the FDA for the treatment of MCI or mild dementia due to AD (Rabinovici, 2021). In the setting of drug treatment, PET quantification could be used to augment the reliability of qualitative methods such as visual reads for determining amyloid status. PET quantification may in the future be used to gauge treatment response or manage dose titration and treatment duration, as was done in a recent Phase 2 study of the anti-amyloid antibody donanemab (Mintun et al., 2021). We suggest rPOP could be used in both clinical

trial and research settings to obtain reliable, quantification-based amyloid status, especially when lacking a structural MRI. Employing rPOP in place of an MRI-based processing could reduce selection bias in research studies and improve generalizability by not excluding specific participant groups from research studies.

While improving access to quantification, PET-only processing has intrinsic limitations that should be considered when interpreting data. First, severe atrophy may impact the expected tracer distribution, which could result in a sub-optimal warping. Second, very atypical amyloid-PET binding patterns may be less efficiently handled by a PET-only processing relying on templates which largely reflect stereotypical patterns. There is however indication that amyloid-PET patterns are rather homogeneous across clinical phenotypes and ages of onset in sporadic Alzheimer's Disease (Iaccarino et al., 2021; La Joie et al., 2021; Laforce et al., 2014; Lehmann et al., 2013). Finally, the MRI-based approach should still be preferred when available with a sufficient quality given the higher anatomical precision in defining regions and structures that can be used to sample processed PET scans.

The complete source code and files to run rPOP are available at https://github.com/leoiacca/rPOP.

Acknowledgments

The authors wish to thank Susan Landau, Tyler Ward, Alice Murphy and Bill Jagust for the insightful discussions and support. The present study was supported by National Institutes of Health (to RLJ, NIH/NIA K99-AG065501; to GDR NIH/NIA R35-AG072362), Alzheimer's Association (to GDR, ZEN-21-848216; to GDR and LI, SG-21-876655). Dr. Siegel receives research support from the American College of Radiology, Blue Earth Diagnostics, LLC, ImagingAb, Inc. and Progenics Pharmaceuticals; consulting fees from the American College of Radiology, American Medical Foundation for Peer Review & Education, Avid Radiopharmaceuticals, Inc., Capella Imaging, LLC, Curium Pharma, GE Healthcare, Lantheus Medical Imaging, Inc. and the Radiological Society of North America; and lecture honoraria from Siemens Healthineers (spouse). Dr. Nosheny receives funding from the National Institute of Aging, Genentech Inc., California Department of Public Health. Dr. Rabinovici receives research support from Avid Radiopharmaceuticals Inc, GE Healthcare, and Life Molecular Imaging via the IDEAS study, and from Genentech. He has received consulting fees from Eisai, Genentech, Johnson & Johnson and Roche. The IDEAS Study and this work were funded by the Alzheimer's Association, the American College of Radiology, Avid Radiopharmaceuticals Inc, GE Healthcare, and Life Molecular Imaging (formerly Piramal Imaging). Data collection and sharing for this project was funded by the Alzheimer's Disease Neuroimaging Initiative (ADNI) (National Institutes of Health Grant U01 AG024904) and DOD ADNI (Department of Defense award number W81XWH-12-2-0012). ADNI is funded by the National Institute on Aging, the National Institute of Biomedical Imaging and Bioengineering, and through generous contributions from the following: AbbVie, Alzheimer's Association; Alzheimer's Drug Discovery Foundation; Araclon Biotech; BioClinica, Inc.; Biogen; Bristol-Myers Squibb Company; CereSpir, Inc.; Cogstate; Eisai Inc.; Elan Pharmaceuticals, Inc.; Eli Lilly and Company; EuroImmun; F. Hoffmann-La Roche Ltd and its affiliated company Genentech, Inc.; Fujirebio; GE Healthcare; IXICO Ltd.; Janssen Alzheimer Immunotherapy Research & Development, LLC.; Johnson & Johnson Pharmaceutical Research & Development LLC.; Lumosity; Lundbeck; Merck & Co., Inc.; Meso Scale Diagnostics, LLC.; NeuroRx Research; Neurotrack Technologies; Novartis Pharmaceuticals Corporation; Pfizer Inc.; Piramal Imaging; Servier; Takeda Pharmaceutical Company; and Transition Therapeutics. The Canadian Institutes of Health Research is providing funds to support ADNI clinical sites in Canada. Private sector contributions are facilitated by the Foundation for the National Institutes of Health (www.fnih.org). The grantee organization is the Northern California Institute for Research and Education, and the study is coordinated by the Alzheimer's Therapeutic Research Institute at the University of Southern California. ADNI data are disseminated by the Laboratory for Neuro Imaging at the University of Southern California.

CRediT author statement

Leonardo Iaccarino: Conceptualization, Data curation, Formal analysis, Investigation, Methodology, Software, Validation, Visualization, Writing - original draft, Writing - review & editing

Renaud La Joie: Conceptualization, Investigation, Methodology, Validation, Visualization, Writing - review & editing

Robert Koeppe: Conceptualization, Methodology, Validation, Writing - review & editing

Barry A. Siegel: Funding acquisition, Writing - review & editing

Bruce E. Hillner: Funding acquisition, Writing - review & editing

Constantine Gatsonis: Data curation, Funding acquisition, Project administration, Writing - review & editing

Rachel A. Whitmer: Funding acquisition, Writing - review & editing

Maria C. Carrillo: Funding acquisition, Writing - review & editing

Charles Apgar: Data curation, Funding acquisition, Project administration, Writing - review & editing

Monica R. Camacho: Data curation, Project administration, Writing - review & editing

Rachel Nosheny: Data curation, Funding acquisition, Investigation, Project administration, Writing - review & editing

Gil D. Rabinovici: Conceptualization, Funding acquisition, Investigation, Project administration, Resources, Supervision, Validation, Writing - review & editing

Supplementary materials

Supplementary material associated with this article can be found, in the online version, at doi:10.1016/j.neuroimage.2021.118775.

References

Akamatsu, G., Ikari, Y., Ohnishi, A., Nishida, H., Aita, K., Sasaki, M., Yamamoto, Y., Sasaki, M., Senda, M., 2016. Automated PET-only quantification of amyloid deposition with adaptive template and empirically pre-defined ROI. Phys. Med. Biol. 61, 5768–5780. doi:10.1088/0031-9155/61/15/5768.

Avgerinos, K.I., Ferrucci, L., Kapogiannis, D., 2021. Effects of monoclonal antibodies against amyloid-β on clinical and biomarker outcomes and adverse event risks: a systematic review and meta-analysis of phase III RCTs in Alzheimer's disease. Ageing Res. Rev. 68, 101339. doi:10.1016/j.arr.2021.101339.

Bejanin, A., La Joie, R., Landeau, B., Belliard, S., de La Sayette, V., Eustache, F., Desgranges, B., Chételat, G., 2019. Distinct interplay between atrophy and hypometabolism in Alzheimer's versus semantic dementia. Cereb. Cortex 29, 1889–1899. doi:10.1093/cercor/bhy069.

Bourgeat, P., Villemagne, V.L., Dore, V., Brown, B., Macaulay, S.L., Martins, R., Masters, C.L., Ames, D., Ellis, K., Rowe, C.C., Salvado, O., Fripp, J.AIBL Research Group, 2015. Comparison of MR-less PiB SUVR quantification methods. Neurobiol. Aging 36 (Suppl 1), S159–S166. doi:10.1016/j.neurobiolaging.2014.04.033.

Cox, R.W., 1996. AFNI: software for analysis and visualization of functional magnetic resonance neuroimages. Comput. Biomed. Res. 29, 162–173. doi:10.1006/cbmr.1996.0014.

Cox, R.W., Hyde, J.S., 1997. Software tools for analysis and visualization of fMRI data. NMR Biomed. 10, 171–178. doi: 10.1002/(sici)1099-1492(199706/08)10:4/5<171::aid-nbm453>3.0.co;2-l.

Dore, V., Bourgeat, P., Villemagne, V.L., Fripp, J., Macaulay, L., Masters, C.L., Ames, D., Rowe, C.C., Salvado, O., 2016. CapAIBL: automated reporting of cortical PET quantification without need of MRI on brain surface using a patch-based method. In: Wu, G., Coupé, P., Zhan, Y., Munsell, B.C., Rueckert, D. (Eds.), Patch-Based Techniques in Medical Imaging, Lecture Notes in Computer Science. Springer International Publishing, Cham, pp. 109–116. doi:10.1007/978-3-319-47118-1_14.

Edison, P., Carter, S.F., Rinne, J.O., Gelosa, G., Herholz, K., Nordberg, A., Brooks, D.J., Hinz, R., 2013. Comparison of MRI based and PET template based approaches in the quantitative analysis of amyloid imaging with PIB-PET. Neuroimage 70, 423–433. doi:10.1016/j.neuroimage.2012.12.014.

Fripp, J., Bourgeat, P., Raniga, P., Acosta, O., Villemagne, V., Jones, G., O'keefe, G., Rowe, C., Ourselin, S., Salvado, O., 2008. MR-less high dimensional spatial normalization of 11C PiB PET images on a population of elderly, mild cognitive impaired and Alzheimer disease patients. Med. Image Comput. Comput. Assist. Interv. 11, 442–449. doi:10.1007/978-3-540-85988-8_53.

Iaccarino, L., La Joie, R., Edwards, L., Strom, A., Schonhaut, D.R., Ossenkoppele, R., Pham, J., Mellinger, T., Janabi, M., Baker, S.L., Soleimani-Meigooni, D., Rosen, H.J., Miller, B.L., Jagust, W.J., Rabinovici, G.D., 2021. Spatial relationships between molecular pathology and neurodegeneration in the Alzheimer's disease continuum. Cereb. Cortex 31, 1–14. doi:10.1093/cercor/bhaa184.

Jagust, W., 2018. Imaging the evolution and pathophysiology of Alzheimer disease. Nat. Rev. Neurosci. 19, 687–700. doi:10.1038/s41583-018-0067-3.

Jagust, W.J., Landau, S.M., Koeppe, R.A., Reiman, E.M., Chen, K., Mathis, C.A., Price, J.C., Foster, N.L., Wang, A.Y., 2015. The Alzheimer's disease neuroimaging initiative 2 PET Core: 2015. Alzheimers Dement. 11, 757–771. doi:10.1016/j.jalz.2015.05.001.

Kang, S.K., Seo, S., Shin, S.A., Byun, M.S., Lee, D.Y., Kim, Y.K., Lee, D.S., Lee, J.S., 2018. Adaptive template generation for amyloid PET using a deep learning approach. Hum. Brain Mapp. 39, 3769–3778. doi:10.1002/hbm.24210.

Klunk, W.E., Engler, H., Nordberg, A., Wang, Y., Blomqvist, G., Holt, D.P., Bergström, M., Savitcheva, I., Huang, G., Estrada, S., Ausén, B., Debnath, M.L., Barletta, J., Price, J.C., Sandell, J., Lopresti, B.J., Wall, A., Koivisto, P., Antoni, G., Mathis, C.A., Långström, B., 2004. Imaging brain amyloid in Alzheimer's disease with Pittsburgh compound-B. Ann. Neurol. 55, 306–319. doi:10.1002/ana.20009.

Klunk, W.E., Koeppe, R.A., Price, J.C., Benzinger, T.L., Devous, M.D., Jagust, W.J., Johnson, K.A., Mathis, C.A., Minhas, D., Pontecorvo, M.J., Rowe, C.C., Skovronsky, D.M., Mintun, M.A., 2015. The Centiloid project: standardizing quantitative amyloid plaque estimation by PET. Alzheimer's Dement. 11, 1–15. doi:10.1016/j.jalz.2014.07.003, e4.

La Joie, R., Ayakta, N., Seeley, W.W., Borys, E., Boxer, A.L., DeCarli, C., Doré, V., Grinberg, L.T., Huang, E., Hwang, J.-.H., Ikonomovic, M.D., Jack, C., Jagust, W.J., Jin, L.-.W., Klunk, W.E., Kofler, J., Lesman-Segev, O.H., Lockhart, S.N., Lowe, V.J., Masters, C.L., Mathis, C.A., McLean, C.L., Miller, B.L., Mungas, D., O'Neil, J.P., Olichney, J.M., Parisi, J.E., Petersen, R.C., Rosen, H.J., Rowe, C.C., Spina, S., Vemuri, P., Villemagne, V.L., Murray, M.E., Rabinovici, G.D., 2019. Multisite study of the relationships between antemortem [11C]PIB-PET Centiloid values and postmortem measures of Alzheimer's disease neuropathology. Alzheimer's Dement. 15, 205–216. doi:10.1016/j.jalz.2018.09.001.

La Joie, R., Visani, A.V., Lesman-Segev, O.H., Baker, S.L., Edwards, L., Iaccarino, L., Soleimani-Meigooni, D.N., Mellinger, T., Janabi, M., Miller, Z.A., Perry, D.C., Pham, J., Strom, A., Gorno-Tempini, M.L., Rosen, H.J., Miller, B.L., Jagust, W.J., Rabinovici, G.D., 2021. Association of APOE4 and clinical variability in alzheimer disease with the pattern of Tau- and amyloid-PET. Neurology 96, e650–e661. doi:10.1212/WNL.0000000000011270.

Laforce, R., Tosun, D., Ghosh, P., Lehmann, M., Madison, C.M., Weiner, M.W., Miller, B.L., Jagust, W.J., Rabinovici, G.D., 2014. Parallel ICA of FDG-PET and PiB-PET in three conditions with underlying Alzheimer's pathology. NeuroImage: Clin. 4, 508–516. doi:10.1016/j.nicl.2014.03.005.

Lehmann, M., Ghosh, P.M., Madison, C., Laforce, R., Corbetta-Rastelli, C., Weiner, M.W., Greicius, M.D., Seeley, W.W., Gorno-Tempini, M.L., Rosen, H.J., Miller, B.L., Jagust, W.J., Rabinovici, G.D., 2013. Diverging patterns of amyloid deposition and hypometabolism in clinical variants of probable Alzheimer's disease. Brain 136, 844–858. doi:10.1093/brain/aws327.

Li, X., Morgan, P.S., Ashburner, J., Smith, J., Rorden, C., 2016. The first step for neuroimaging data analysis: DICOM to NIfTI conversion. J. Neurosci. Methods 264, 47–56. doi:10.1016/j.jneumeth.2016.03.001.

Lilja, J., Leuzy, A., Chiotis, K., Savitcheva, I., Sörensen, J., Nordberg, A., 2019. Spatial normalization of 18F-flutemetamol PET images using an adaptive principal-component template. J. Nucl. Med. 60, 285–291. doi:10.2967/jnumed.118.207811.

Lundqvist, R., Lilja, J., Thomas, B.A., Lötjönen, J., Villemagne, V.L., Rowe, C.C., Thurfjell, L., 2013. Implementation and validation of an adaptive template registration method for 18F-flutemetamol imaging data. J. Nucl. Med. 54, 1472–1478. doi:10.2967/jnumed.112.115006.

Mintun, M.A., Lo, A.C., Duggan Evans, C., Wessels, A.M., Ardayfio, P.A., Andersen, S.W., Shcherbinin, S., Sparks, J., Sims, J.R., Brys, M., Apostolova, L.G., Salloway, S.P., Skovronsky, D.M., 2021. Donanemab in early Alzheimer's disease. N. Engl. J. Med. 384, 1691–1704. doi:10.1056/NEJMoa2100708.

Nosheny, R.L., Camacho, M.R., Jin, C., Neuhaus, J., Truran, D., Flenniken, D., Ashford, M., Carrillo, M.C., Fargo, K.N., Hendrix, J., Hanna, L., Rabinovici, G., Maruff, P., Mackin, R.S., Weiner, M.W., 2020. Validation of online functional measures in cognitively impaired older adults. Alzheimers Dement. 16, 1426–1437. doi:10.1002/alz.12138.

Pegueroles, J., Montal, V., Bejanin, A., Vilaplana, E., Aranha, M., Santos-Santos, M.A., Alcolea, D., Carrió, I., Camacho, V., Blesa, R., Lleó, A., Fortea, J.Alzheimer Disease Neuroimaging Initiative, Australian Imaging, Biomarkers and Lifestyle Research Group, 2021. AMYQ: An index to standardize quantitative amyloid load across PET tracers. Alzheimers Dement. 17, 1499–1508. doi:10.1002/alz.12317.

Rabinovici, G.D., 2021. Controversy and progress in alzheimer's disease - FDA approval of Aducanumab. N. Engl. J. Med. 385, 771–774. doi:10.1056/NEJMp2111320.

Rabinovici, G.D., Gatsonis, C., Apgar, C., Chaudhary, K., Gareen, I., Hanna, L., Hendrix, J., Hillner, B.E., Olson, C., Lesman-Segev, O.H., Romanoff, J., Siegel, B.A., Whitmer, R.A., Carrillo, M.C., 2019. Association of amyloid positron emission tomography with subsequent change in clinical management among medicare beneficiaries with mild cognitive impairment or dementia. JAMA 321, 1286. doi:10.1001/jama.2019.2000.

Royse, S.K., Minhas, D.S., Lopresti, B.J., Murphy, A., Ward, T., Koeppe, R.A., Bullich, S., DeSanti, S., Jagust, W.J., Landau, S.M.Alzheimer's Disease Neuroimaging Initiative, 2021. Validation of amyloid PET positivity thresholds in centiloids: a multisite PET study approach. Alzheimers Res. Ther. 13, 99. doi:10.1186/s13195-021-00836-1.

Thal, D.R., Rüb, U., Orantes, M., Braak, H., 2002. Phases of A beta-deposition in the human brain and its relevance for the development of AD. Neurology 58, 1791–1800. doi:10.1212/wnl.58.12.1791.

Villemagne, V.L., Doré, V., Burnham, S.C., Masters, C.L., Rowe, C.C., 2018. Imaging tau and amyloid-β proteinopathies in Alzheimer disease and other conditions. Nat. Rev. Neurol. 14, 225–236. doi:10.1038/nrneurol.2018.9.